



ISSN: 2350-0328

**International Journal of Advanced Research in Science,
Engineering and Technology**

Vol. 4, Issue 7, July 2017

Review on Intravascular Ultrasound (IVUS) Image Detection

K.V.Archana, Dr.R.Vanithamani

Assistant Professor ,Electronics and Communication Engineering, Faculty of Engineering, Avinashilingam Institute for Home Science and Higher Education for Women- University, India.

Associate Professor, Biomedical and Instrumentation Engineering, Faculty of Engineering, Avinashilingam Institute for Home Science and Higher Education for Women- University, India.

ABSTRACT: Visualization of the blood vessels can provide valuable morphological information for diagnosis and therapy strategies for cardiovascular disease. Intravascular ultrasound (IVUS) is able to delineate internal structures of vessel wall with fine spatial resolution. In this paper, we review recently developed image processing methods for the detection of media–adventitia and luminal borders in IVUS images acquired with different transducers operating at frequencies ranging from 20 to 45 MHz. We discuss methodological challenges, lack of diversity in reported datasets, and weaknesses of quantification metrics that make IVUS segmentation still an open problem despite all efforts

KEY WORDS: Intravascular ultrasound (IVUS), lumen, media–adventitia (MA)

I. INTRODUCTION

Intravascular Ultrasound (IVUS) is an invasive, catheter-based imaging modality that provides cross sectional images of the interior of a blood vessel in real time and at video frame rates. For studies of vessel morphology, plaque characterization, and other purposes requiring 3-D imagery, the transducer-bearing catheter can be gradually withdrawn through the vessel during recording. Moreover, it enables the monitoring of regression and progression of plaques by measuring changes over time of the atheroma volume within the vessel wall, especially when evaluating new pharmacological compounds. Besides, for chronic disease such as atherosclerosis that may reoccur after balloon angioplasty, atherectomy, stenting, or bypass surgery, the accurate diagnosis of vulnerable plaques [3]–[7] is critical. In brief, *what makes atherosclerosis one of the deadliest disease is not the stenosis alone but failure in detection and proper treatment of the vulnerable plaques that will lead to myocardial infarction.* This point has motivated researchers to develop novel imaging modalities such as IVUS, optical coherence tomography (OCT) [8], or near-infrared signals (NIR) [9] to characterize atherosclerotic plaque components and identify vulnerable ones.

A. Specificities of IVUS Images

Angiography is the only system routinely used in all PCI procedures. It provides immediate visualization of stenoses and guides interventional cardiologists to advance and deploy balloons and stents. However, it suffers from the lack of adequate geometrical and pathological information on plaque burden size and composition. So far, IVUS remains the most favourable imaging modality for coronary plaques for the following reasons.

- 1) It provides real-time cross-sectional gray scale images of the arterial wall, including morphological and pathological structures. Image resolution and signal penetration are sufficient to allow precise tomographic assessment of the coronaries.
- 2) IVUS gray scale images combined with the processing of radio frequency backscattered signals can be employed for further characterization of plaques and the identification of vulnerable ones [10].
- 3) Interventional cardiologists can make therapeutic decisions from IVUS images, such as:
 - a) the need for further treatment (angioplasty, stent implantation, and bypass);
 - b) the exact spatial location for angioplasty and stent implantation;
 - c) the evaluation of the outcome of an angioplasty or stenting procedure
 - d) the need for aggressive management of risk factors prior to onset of symptoms and advanced disease state;
 - e) the predictors of transplant coronary artery disease.

B. IVUS Acquisition Systems

The IVUS acquisition system consists of a catheter, a pullback device, and a scanning console.

1) IVUS Catheter: The IVUS catheter carries an ultrasound transducer that can be combined with an inflatable balloon, with or without a stent, for imaging assistance and expansion of narrowed areas, as illustrated in Fig. 1. The IVUS catheter is 150 cm long, and has a tip size of 3.2–3.5 F (1.2–1.5 mm) that can go through 5–6 F guiding catheter. It may be used to visualize over 15 cm of a coronary artery. The imaging field goes up to 15–20 mm, well enough for coronary arteries, ranging from 4 to 5mm in diameter on average at the level of the left main artery down to 2mm in the smallest segment considered for therapeutic intervention (balloon angioplasty and stenting). The catheter is typically advanced within the femoral artery toward coronary arteries and site of occlusion under angiogram guidance. The catheter is visible in angiographic images and is advanced along with a guide wire. The guide wire rail is positioned next to the catheter plastic sheath, as in Fig. 1(b), or within its centre, as in Fig. 1(c). The advantage of the latter design is that there is no guide wire artifact in the reconstructed gray scale ultrasound images, but at the cost of usually stiffer, thicker, and less flexible catheters.

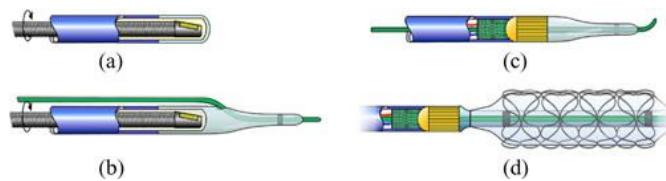


Fig. 1. Schematic of four different types of imaging catheters.

(a) Catheter without guide wire rail. (b) Catheter with a guide wire rail on the side. (c) Catheter with a guide wire rail at its center. (d) Catheter with a guide wire rail at its center, an inflatable balloon, and a stent.

Reference: http://ee.isikun.edu.tr/research.asp-page = projects_files.

2) IVUS Transducer: Currently, there are two types of IVUS transducers commercially available regardless of their nominal center frequencies. The main difference relies in the transmit and receive modes for monitoring ultrasound signals, which are illustrated in Fig. 2. The first system, illustrated in Fig. 2(a), uses a single-element mechanically rotating focused IVUS transducer that rotates at approximately 1800 revolutions/min. For a 40-MHz transducer, the axial and lateral resolutions of the beam are about 80–100 and 200–250 μm , respectively. The transducer sends an ultrasound pulse and receives the backscattered signals. The transducer is surrounded by a plastic sheath and a syringe is used to flush saline water inside the sheath to remove air bubbles and obtain high-quality IVUS images.

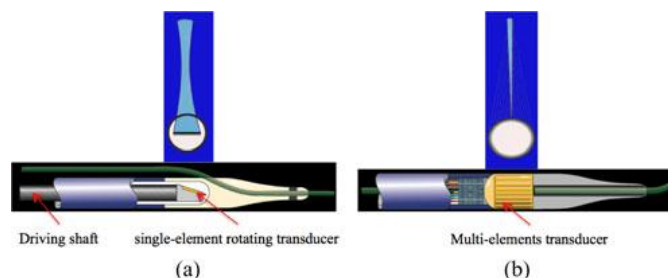


Fig. 2. (a) Single-element mechanically rotating focused IVUS transducer and its beam shape. (b) Multi-element phased-array IVUS transducer and its beam shape.

The second system, illustrated in Fig. 2(b), uses a multi element phased-array transducer. An electronic board controls a subset of elements to send several ultrasound pulses at once and receive the backscattered signals. These circular

array systems use synthetic aperture processing to produce images with higher lateral resolution than single-element transducers.

3) Catheter Pullback Device: The catheter is first manually advanced to the distal end of the coronary (typically after the stenoses location) and is then pulled back, manually or with an automatic pullback system, at a speed of 0.5–1 mm/s.

4) IVUS Scanning Consoles: A scanning console carries a computer that is used for post processing and storage of recorded IVUS data. A cable from the end of the pullback device is connected, via a dedicated port, with a computer for data processing. During the catheterization procedure, the clinician uses a keyboard and functional buttons to enter the patient information, determine the percentage of stenoses, and apply image processing and possibly tissue characterization techniques to better understand and evaluate atherosclerotic plaques.

C. IVUS Image Formation and Display

IVUS transducers operate at different frequencies, depending on the manufacturer. Fig. 3 displays the schematic of an artery, an IVUS catheter, and four distinct IVUS image frames acquired with transducers with different centre frequencies.

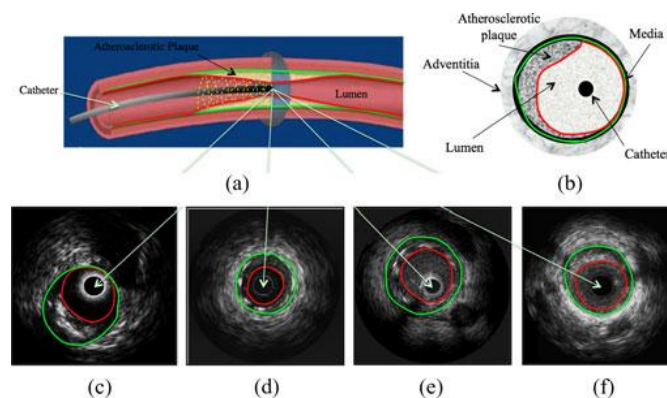


Fig. 3. (a) Schematic of an artery, catheter, atherosclerotic plaque, and IVUS image cross section (reference: <http://www.bmj.com>). (b) Cross-sectional anatomy of the arterial wall. Four distinct IVUS frames acquired with (c) 20-MHz, (d) 30-MHz, (e) 40-MHz, and (f) 45-MHz transducers. Green and red borders represent the vessel wall (MA) and lumen (intima) borders, respectively. The yellow dashed line depicts the trajectory of transducer scan lines.

As illustrated, at higher centre frequency, spatial resolution is improved, at the cost of more scattering from red blood cells inside the lumen. It is worth mentioning that the axial and lateral resolutions depend on the transducer center frequency and beam width, respectively.

During acquisition, IVUS backscattered radiofrequency (RF) signals that are continuous-time real-valued and band-limited signals, $x(t)$, are digitized $x(nTs) = xn$ at periodic time intervals of $Ts = f_s^{-1}$ and stored in the hard disk of a computer. f_s is the sampling rate of the digitizing board and may vary from one system to another. Once the IVUS backscattered signals are digitized, numbers of steps need to be taken in order to convert digitized RF signals into typical IVUS gray scale images. First, the envelope of each RF signals (A-line) is computed to generate a corresponding analytical signal [12]. This is followed by decimation and interpolation along the axial and lateral directions, respectively. Log compression is also used to enhance image quality followed by a quantization.

D. IVUS Image Artifacts

IVUS images may suffer from severe acquisition artifacts.

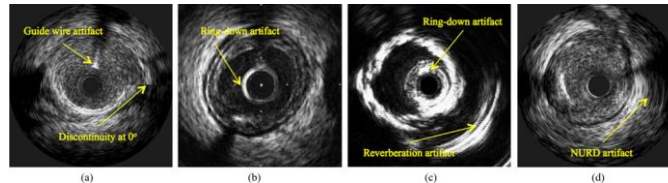


Fig. 4. IVUS image artifacts. (a) Guide wire artifact and discontinuity artifact at 0° . (b) Ring-down artifact. (c) Ring-down artifact and reverberation artifact. (d) NURD artifact. Calibration markers (small white squares) in (b) are used for measurements.

We can cite five main artifacts: presence of the guide wire, ring-down, nonuniform rotational distortion (NURD), reverberation, and discontinuity at 0° in the Cartesian domain. When a guide wire rail is designed along with a plastic sheath of the catheter, it obstructs the propagation of ultrasound signals, resulting in shadowing behind the guide wire, as illustrated in Fig. 4(a). The second artifact arises from the repetitive reflections of the ultrasound signal from the surface of the transducer because of impedance mismatch, as illustrated in Fig. 4(b). The NURD artifact is due to a mechanical glitch in the driving shaft or the binding of the catheter in curved arteries, as illustrated in Fig. 4(d). The fourth artifact, known as reverberation, corresponds to oscillations of the ultrasound signals between the transducers and the arc of calcified plaques, which causes multiple appearances of calcified arcs, as illustrated in Fig. 4(c). The last artifact corresponds to a discontinuity of tissue appearance at 0° in the Cartesian domain due to the spiral trajectory of the transducer as well as severe catheter or heart motions, as illustrated in Fig. 4(a).

E. In Vivo Data Collection

Generally, an IVUS catheter is advanced into the left or right coronary artery and possibly in some side branches on a guide wire coming out of a guiding catheter inserted in the femoral artery. Acquisition of cross-sectional ultrasound images of the right coronary arteries (RCA), left anterior descending (LAD), and left circumflex (LCX) coronary arteries can be performed with a rotating single-element transducer or a phased array transducer. The catheter pullback speed varies between 0.5 and 1 mm/s and the frame rate can be set to 30–60 frames/s.

F. Image Processing Challenges

During a catheterization procedure, hundreds to thousands of IVUS images are recorded. Therefore, automatic detection of the vessel wall [media–adventitia (MA)] and luminal borders is required to quantify the degree of stenoses and measure the luminal area in which blood flows. The lumen border is at the innermost surface of atherosclerotic plaques. Since ultrasound signals are progressively weakened with depth, time gain compensation (TGC) can be applied to compensate for this, as illustrated in Fig. 5. The vessel wall border, also called the external elastic membrane (EEM) border, is a contour drawn at the interface between the media and the adventitia. Made of smooth muscle cells, the media does not reflect the ultrasound signal and appears as a dark ring. Adventitia is the outer layer of an artery, formed of sheets layers that are hyperechogenic and appear as a bright region.

Generally speaking, detection of vessel wall borders is less difficult than that of lumen borders since the vessel media consists of smooth muscle cells and does not reflect ultrasound signals. It appears as a dark region on IVUS images, which can be used as a marker to detect the vessel wall. In contrast, due to high scattering from red blood cells inside the lumen, the detection of the luminal border is more challenging, especially when a high-frequency transducer is used. Comparing IVUS ultrasound probes, the lumen border is more easily detected in images acquired with a 64-element phased-array 20-MHz transducer than with a single-element mechanically rotating 45-MHz transducer, as illustrated in Fig.3.

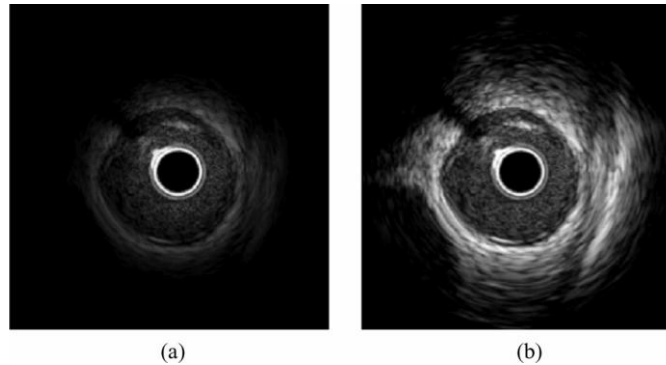


Fig. 5. IVUS gray scale image (a) without TGC adjustment and (b) with TGC adjustment.

In any case, clinical applications of automated segmentation methods have seen limited success due to several intrinsic artifacts (presence of the guide wire, presence of calcified plaques, presence of side branches, motion of the catheter and the heart) and extrinsic parameters (such as manual setting of TGC). For example, the presence of the guide wire, calcified plaques, and side branches significantly affects an algorithm performance, particularly when deformable models are employed. On the other hand, variability among system specifications or changes of acquisition parameters by an expert would lead to inconsistency among datasets so that supervised techniques or those that rely on statistical properties of gray level intensities may not perform efficiently.

In this paper, we review segmentation algorithms that detect either both borders simultaneously or one of them. To tackle the segmentation problem, researchers have developed several algorithms, employing different techniques such as graph searching, gradient-driven methods with dynamic programming, and deformable models in combination with statistical properties of gray scale values corresponding to blood and non blood regions, statistical shape models, probabilistic approaches, edge-enhancement frameworks along with active contours, or multiscale techniques, for example. We distinguished three main families of approaches: 1) direct detection of border(s); 2) blood speckle reduction (i.e., spatiotemporal filtering) as a preprocessing step prior to border detection; and 3) supervised classification [e.g., support vector machine (SVM)] of blood versus non blood regions by extracting appropriate spatial/temporal/spectral features.

II. DIRECT DETECTION OF BORDER(S)

A. Edge-Tracking and Gradient-Based Techniques

The interactions of IVUS signal with the blood–tissue interface and smooth muscle cells in media give rise to typical edge patterns that could be used to distinguish lumen and MA contours, respectively. In practice, these patterns seldom embody clean borders due to scattering effects within the lumen, discontinuity in intensity values, drops in edge reflections, noise. Hence, further refinement (e.g., smoothing for noise reduction) and hybrid algorithms were designed to assemble edge features into desirable target boundaries. The IVUS segmentation techniques that deploy such image descriptors usually require precise initialization and rely on an energy minimization framework.

The very first work on IVUS border detection from Herrington *et al.* [13] developed a semi automated algorithm based on such principle. Later, Sonka *et al.* [14] introduced one of the earliest comprehensive works on the detection of internal and external elastic laminae borders as well as lumen borders. The internal and external elastic laminae borders refer to the inner and outer layers of the media, which consist of smooth muscle cells. Normally, the MA border can be drawn anywhere between these two borders (within the corresponding hypo echoic region). After removing the calibration markers, regions of interest (ROIs) were interactively selected and Sobel-like edge detectors were applied on sub images to construct laminae and lumen border graphs. A heuristic graph search technique [15], [16] was then performed deploying two distinct cost functions to detect the borders. The key point for precise identification of borders was to define appropriate cost functions for each border by incorporating *a priori* knowledge such as shape models and edge patterns. The results demonstrated good correlation between manual and automated lumen borders ($r = 0.96$), plaques ($r = 0.95$), and stenoses areas ($r = 0.93$). Although the presented technique required some user interaction and was only applied on *in vitro* images using circulating saline water, where there was not much scattering



ISSN: 2350-0328

International Journal of Advanced Research in Science, Engineering and Technology

Vol. 4, Issue 7 , July 2017

in the lumen area compared to *in vivo* images, the results were encouraging and this study raised attentions toward this particular problem. An extended version of this approach using a different cost function and fully 3-D graph search has been presented in [17].

With a similar type of approach, the authors in [18] and [19] presented a semi-automated methodology using dynamic programming to find the optimal path within the vessel and detect both MA and lumen borders in polar coordinates from delineated contours. The minimal path search was performed between end points interactively selected in reconstructed longitudinal images at the intersection of two perpendicular cut planes. The results were validated using both tubular phantom data and *in vivo* images acquired with a 30-MHz transducer [18]. They studied inter- and intra observer variability and showed high consistency of the method. They later evaluated the performance of the segmentation by comparing to histological images [20]. The algorithm performance was further refined and correlation between manual and automated traced contours was improved from ($r = 0.91$) to ($r = 0.98$) by employing electrocardiogram (ECG)-gated images [21]. The main limitations were related to non-uniform transducer rotation and high curvature of the arterial vessel shape that created distortions in planar images. In addition, accurate positioning of an individual transverse plane in longitudinal sections was crucial and could affect the quality of the segmentation. A similar semi-automated knowledge guided approach was also proposed by the authors in [22].

Meier *et al.* [23] proposed a fully automated segmentation method for the detection of both MA and lumen borders through the enhancement of image continuity along the circumferential direction in polar coordinates and speckle noise reduction by applying iterative nonlinear spatial median filters. Three different segmentation techniques were applied to detect the lumen borders: 1) thresholding of gray scale gradient maps obtained by convolving the polar image with gradient kernels in the radial direction; 2) adaptive region growing from a luminal seed point (after the detection of the catheter); and 3) deformation of a gradient-based parametric deformable model to search for connected outline points and detect the MA border. Post processing was required to remove remaining outliers and refine the final segmentation. Two distinct datasets consisting of 77 and 28 *in vivo* collected IVUS frames acquired with a single-element 30-MHz transducer were then used for the detection of lumen and MA borders, respectively. The authors in [24] proposed a modified image cost function, combining gradient and variance of gray scale intensities, which was less sensitive to noise and employed circular dynamic programming for the detection of the MA borders. The presented algorithm required manual initialization of ROI in the first frame of analysis. Analogous to the method in [23], Schmauder *et al.* [25] used dedicated preprocessing (i.e., median filtering and histogram equalization) to remove catheter markers and scaling grids. They started with an initialized contour to confine the segmentation process within ROI. A radial search procedure was performed, optimizing an energy functional formulated as a weighted linear combination of an edge detector (first derivative of a Gaussian operator), an appearance feature (mean value of intensity measured within sliding windows), and a smoothing term. A multi-temperature simulated annealing optimization was then used to minimize the energy functional and detect the lumen border. The performance of the algorithm was evaluated using 160 frames collected from five patients using a single-element 30-MHz transducer.

B. Active Contour-Based Techniques

Active contours have been widely used in many medical image segmentation applications and most of the IVUS studies adopted the traditional formulation of a parametric snake. Rather than implicit shape surface representation to retrieve lumen and/or MA boundaries. Parametric model formulation is more intuitive and better IVUS border detection applications since the topology of different boundaries is simple and underlying parameterization remains simple and computationally efficient. The tradeoff of using parametric representations relies in the fact that it is more sensible to initial conditions because of nonconvexity of the energy functional and the need for advection forces. Due to intrinsic non-vessel image features (presence of guide wire, calcified plaques, side branches, motion artifacts from the catheter and the heart) and image variability due to extrinsic parameters (system parameter specifications such as TGC and compression of the dynamic range), the vessel borders are not well distinguished in IVUS image which hinders the direct use of a classical deformable model. Moreover, fine tuning of parameters and proper initialization are required when ordinary features such as image gradient and intensity, which are sensitive to noise, are employed. Hence, several approaches have been proposed to overcome these drawbacks by modifying the energy terms or incorporating pre-processing techniques prior to the use of a deformable model. In addition, they modified the definition of the bias of neurons, incorporating image characteristics as *a priori*, to overcome possible distortions in textural patterns due to the presence of arcs of calcified plaques and detected both borders. The user only needed to initialize



ISSN: 2350-0328

International Journal of Advanced Research in Science, Engineering and Technology

Vol. 4, Issue 7, July 2017

lumen and MA borders in the very first frames and resulting detected borders then were automatically employed as initial contours for subsequent frames.

As an alternative automated approach, Kovalski *et al.* [24] removed the elasticity term from the internal energy. To control the smoothness of the contour, they introduced an *a priori* on the final desired shape via regularization along longitudinal direction, and a “balloon” force to control point motion only along radial directions. The contours evolved toward features of interest driven by intensity-based external forces. Finally, they extended the algorithm to 3-D for the automatic detection of MA and lumen borders. The results demonstrated high correlation for lumen and MA borders, respectively, when comparing to manual tracing. The authors in [23] also developed a semi automated 3-D segmentation framework called the active surface model, which was an extension of a 2-D digital dynamic model (DDM) technique [23], for the detection of both borders. The internal force comprised distinct tangential and radial components derived from corresponding transverse and longitudinal edge vectors. The external force was based on the gradient of a 3-D potential field defined by convolving the image volume with a 3-D Sobel-like kernel. A damping force was used to control the convergence of the model to its final shape. The algorithm required user intervention to initialize the template every other ten frames. The results demonstrated robust segmentation with negligible variability. Later, in a comprehensive study [23], the performance of the algorithm was evaluated against more computationally efficient 3-D active surface algorithm using a so-called neighbourhood-search model.

III. BLOOD NOISE REDUCTION ALGORITHMS

To ease IVUS border detection and more specifically the luminal border, different techniques have been developed to either reduce blood speckle appearance or identify the blood pool directly. Some of the works reviewed in the previous section implemented preprocessing techniques such as median and anisotropic diffusion filtering prior to border detection. However, the focus of this section is on algorithms that are entirely dedicated to blood noise reduction (BNR) and blood pool detection (BPD). The term *blood noise* is associated with scattering from red blood cells inside the lumen. To the best of our knowledge, the authors in [20] were the first to employ signal-processing techniques in lateral direction for BNR in IVUS images acquired with a 20-MHz transducer. The framework exploited the Doppler shift in the blood power spectrum which could be teased out from the vessel wall spectrum centered at the zero frequency using a low-pass filter. Simulations and results driven from *in vitro* data demonstrated the effectiveness of the proposed technique. The rationale behind most BNR and BPD algorithms is that blood and plaques embody incoherent and coherent textural patterns along the pullback direction. Therefore, spatiotemporal information provides discriminative features for blood speckle and blood pool and blood noise effects. The authors also presented a BNR algorithm based on the fusion of anisotropic ally diffused filtered images with temporal information and detection of the lumen borders by thresholding of edge images. BPD has also been a subject of few studies where the presence of incoherent blood speckle patterns hindered the assessment of lumen size in IVUS images, especially for images acquired with recently developed ultrahigh-frequency transducers (40MHz and above).

IV. DISCUSSION AND CONCLUSION

The main contribution of this paper is to introduce state-of-the-art IVUS segmentation techniques developed over the past 20 years. Avoiding direct comparison, we rather categorized algorithms into three groups: direct detection of the MA or the lumen borders, classification of luminal and blood pool areas, and blood speckle noise reduction (BNR) methods. Techniques belonging to the first group (direct detection) are usually preferred as they offer instant measurements of lumen and plaque areas, which are required prior to tissue characterization or balloon angioplasty and stent implantation. Although all reviewed algorithms bring specific advantages, they have been only partially successful in clinical setting. For very precise measurements, e.g., plaque progression/ regression studies during pharmacological trials, most of the research laboratories still rely on manually traced borders.

To make these methods usable in clinical setting, an automated adaptation of the algorithms to morphological and pathological textural changes within pullback series of images needs to be provided. Indeed, most of the validation datasets used in the literature comprises frames from distinct parts of pullback series, which do not reflect the needs during catheterization procedures.



Second, in most studies, the gray scale distributions corresponding to blood and non-blood regions are assumed to be separable. This is a reasonable assumption for images acquired with low-frequency transducers (20–30 MHz), and the authors in [63] have shown that, in such a situation, a thresholding-based technique with empirically tuned values outperforms more sophisticated algorithms. However, this assumption is no longer valid for images acquired with transducers (40MHz and above). As we can see, the separation between blood and non-blood intensities vanishes when the transducer center frequency increases from 20 to 45MHz. As more scattering from red blood cells emerges with the increase in the center frequency of the transducer, visual detection of luminal borders becomes impossible without exploiting the longitudinal incoherence of the blood patterns. Finally, there are still no common datasets freely distributed on which different algorithms could be compared.

In conclusion, to drive automated quantification tools to the clinics, more standardization in the validation process, performance metrics, and construction of globally accessible databases consisting of pullbacks of images that imitate all possible scenarios in real catheterization procedures, acquired with different transducer frequencies, are required.

REFERENCES

- [1] E. J. Topol and S. E. Nissen, "Our preoccupation with coronary lumenology. The dissociation between clinical and angiographic findings in ischemic heart disease," *Circulation*, vol. 92, pp. 2333–2342, 1995.
- [2] F.M. Sones and E. K. Shirey, "Cine coronary arteriography," *Mod. Conc.Cardiovasc. Dis.*, vol. 31, pp. 735–738, 1998.
- [3] W. C. Little, "Angiographic assessment of the culprit coronary artery lesion before acute myocardial infarction," *Amer. J. Cardiol.*, vol. 66, pp. 44G–47G, 1990.
- [4] J. E. Muller and G. H. Tofler, "Triggering and hourly variation of onset of arterial thrombosis," *Ann. Epidemiol.*, vol. 2, pp. 393–405, 1992.
- [5] E. Falk, "Why do plaques rupture?," *Circulation*, vol. 86, pp. III30–III42, 1992.
- [6] P. Libby, "Molecular bases of the acute coronary syndromes," *Circulation*, vol. 91, pp. 2844–2850, 1995.
- [7] R. Virmani, A. P. Burke, F. D. Kolodgie, and A. Farb, "Pathology of the thin-cap fibroatheroma: A type of vulnerable plaque," *J. Interven. Cardiol.*, vol. 16, no. 3, pp. 267–272, 2003.
- [8] I. K. Jang, B. E. Bouma, D. H. Kang, S. J. Park, S. W. Park, K. B. Seung, K. B. Choi, M. Shishkov, K. Schlendrof, E. Pomerantsev, S. L. Houser, H. T. Aretz, and G. J. Tearney, "Visualization of coronary atherosclerotic plaques in patients using optical coherence tomography: Comparison with intravascular ultrasound," *J. Amer. Coll. Cardiol.*, vol. 39, pp. 604–609, 2002.
- [9] J. D. Caplan, S. Waxman, R. W. Nesto, and J. E. Muller, "Near-infrared spectroscopy for the detection of vulnerable coronary artery plaques," *J. Amer. Coll. Cardiol.*, vol. 47, pp. C92–C96, 2006.
- [10] G. W. Stone, A. Maehara, A. J. Lansky, B. de Bruyne, E. Cristea, G. S. Mintz, R. Mehran, J. McPherson, N. Farhat, S. P. Marso, H. Parise, B. Templin, R. White, Z. Zhang, and P. W. Serruys, "A prospective natural history study of coronary atherosclerosis," *N. Engl. J. Med.*, no. 364, pp. 226–235, 2011.
- [11] ACC/AHA/SCAI Writing Committee, "American College of Cardiology American Heart Association Task Force on practice guidelines," *J. Amer. Coll. Cardiol.*, vol. 47, no. 1, pp. e1–e121, 2006.
- [12] A. V. Oppenheim and R. W. Schaffer, *Discrete-Time Signal Processing*, 2nd ed. Englewood Cliffs, NJ: Prentice-Hall, 1998.
- [13] D. M. Herrington, T. Johnson, P. Santago, and W. E. Sydner, "Semiautomated boundary detection for intravascular ultrasound," in *Proc. Comput. Cardiol.*, 1992, vol. 192, pp. 103–106.
- [14] M. Sonka, X. Zhang, M. Siebes, M. S. Bissing, S. C. DeJong, S. M. Collins, and C. R. McKay, "Segmentation of intravascular ultrasound images: Knowledge-based approach," *IEEE Trans. Med. Imag.*, vol. 14, no. 4, pp. 719–732, Dec. 1995.
- [15] M. Sonka, V. Hlavac, and R. Boyle, *Image Processing, Analysis, and Machine Vision*. London, U.K.: Chapman & Hall, 1993.
- [16] N. J. Nilsson, *Problem Solving Methods in Artificial Intelligence*. New York: McGraw Hill, 1971.
- [17] R. Downe, A. Wahle, T. Kovarnik, H. Skalicka, J. Lopez, J. Horak, and M. Sonka, "Segmentation of intravascular ultrasound images using graph search and a novel cost function," in *Proc. Medical Image Computing and Computer Assisted Intervention Workshop on Computer Vision for Intravascular and Intracardiac Imaging*, New York, 2008, pp. 71–79.
- [18] C. von Birgelen, C. Mario, W. Li, J. Schuurbiens, C. Slager, P. de Feyter, P. Serruys, and J. Roelandt, "Morphometric analysis in three-dimensional intracoronary ultrasound: An *in vitro* and *in vivo* study using a novel system for the contour detection of lumen and plaque," *Amer. Heart J.*, vol. 132, no. 3, pp. 516–527, 1996.
- [19] W. Li, C. von Birgelen, C. Di Mario, E. Boersma, E. J. Gussenhoven, N. Van der Putten, and N. Bom, "Semi-automatic detection for volumetric quantification of intracoronary ultrasound," in *Proc. Comput. Cardiology*, Bethesda, MD, 1994, pp. 277–280.
- [20] C. von Birgelen, A. van der Lugt, A. Nicosia, G. S. Mintz, E. J. Gussenhoven, E. de Vrey, M. T. Mallus, J. R. T. C. Roelandt, P. W. Serruys, and P. J. de Feyter, "Computerized assessment of coronary lumen and atherosclerotic plaque dimensions in three-dimensional intravascular ultrasound correlated with histomorphometry," *Amer. J. Cardiol.*, vol. 7, pp. 1202–1209, 1996.
- [21] C. von Birgelen, G. S. Mintz, A. Nicosia, D. P. Foley, W. J. van der Giessen, N. Bruining, S. G. Airtian, J. R. T. C. Roelandt, P. J. de Feyter, and P. W. Serruys, "Electrocardiogram-gated intravascular ultrasound image acquisition after coronary stent deployment facilitates on-line three dimensional reconstruction and automated lumen quantification," *J. Amer. Coll. Cardiol.*, vol. 30, pp. 436–443, 1997.
- [22] J. Dijkstra, G. Koning, J. C. Tuinenburg, P. V. Oemrawsingh, and J. H. G. Reiber, "Automatic border detection in intravascular ultrasound images for quantitative measurements of the vessel, lumen and stent parameters," *Comp. in Cardiol*, pp. 25–28, 2001.
- [23] D. Meier, R. Cothren, D. Vince, and J. Cornhill, "Automated morphometry of coronary arteries with digital image analysis of intravascular ultrasound," *Amer. Heart J.*, vol. 133, no. 6, pp. 681–690, 1997.
- [24] Z. Luo, Y. Wang, and W. Wang, "Estimating coronary artery lumen area with optimization-based contour detection," *IEEE Trans. Med. Imag.*, vol. 22, no. 4, pp. 564–566, Apr. 2003.